Supplementary Information

Investigations of the Stability of Etched or Platinized p-InP(100) Photocathodes for Solar-driven Hydrogen Evolution in Acidic or Alkaline Aqueous Electrolytes

Weilai Yu[1], Matthias H. Richter[1,2], Pakpoom Buabthong[2], Ivan A. Moreno-Hernandez[1], Carlos G. Read[1], Ethan Simonoff[1], Bruce S. Brunschwig[3] and Nathan S. Lewis[1,3*]

[1]Division of Chemistry and Chemical Engineering, [2]Division of Engineering and Applied Science, and [3]Beckman Institute Molecular Materials Resource Center (MMRC), California Institute of Technology, Pasadena CA, 91125

Email: nslewis@caltech.edu

Experimental

Materials

All chemicals and materials were used as received, including sulfuric acid (H_2SO_4, Fisher Scientific, TraceMetal Grade, 93-98%), 1.0 M sulfuric acid solutions (H_2SO_4, VWR Chemicals), potassium hydroxide (KOH, Sigma-Aldrich, semiconductor grade, 99.99 % trace-metal basis), bromine (Br_2, reagent grade, Sigma-Aldrich), ammonia/methanol solution (4.0 M, Sigma-Aldrich), and methanol (CH_3OH, VWR Analytical, ACS, 99.8 %). Deionized water with a resistivity of 18.2 MΩ cm was obtained from a Barnstead Millipore system. Single-side polished, (100)-oriented, Sn-doped (N_d = 1-5×10^{17} cm^{-3}), n-type InP wafers and Zn-doped (N_d = 1-5×10^{17} cm^{-3}), p-type InP wafers were obtained from AXT Inc. Indium foil (0.25 mm thick, 99.99 %) was purchased from VWR International. Nafion (proton-exchange membrane) and Fumasep (anion-exchange membrane) were purchased from the Fuel Cell Store.

Purification of 1.0 M H_2SO_4(aq) and 1.0 M KOH(aq) by pre-electrolysis

Prior to use, the prepared 1.0 M H_2SO_4(aq) and 1.0 M KOH(aq) electrolytes were pre-electrolyzed in a two-compartment electrochemical cell, with the two compartments separated by either a Nafion (acid) or Fumasep (base) membrane. The pre-electrolysis was performed for > 24 h under either a constant > 3 V bias or under a constant current of 6 mA, using two separate carbon cloth or carbon rod electrodes. In some pre-electrolysis experiments of 1.0 M KOH(aq), a Ni foil electrode was also used as the anode for pre-electrolysis of 1.0 M KOH(aq). Only the pre-electrolyzed electrolyte in the cathode compartment was used in subsequent electrochemical measurements. After the electrolysis, H_2O_2 was not detectable in the catholyte, as determined by spectrophotometric analysis using titanium oxalate.[1]

Back contacts to InP electrodes

Ohmic back contacts to n-type InP were obtained by sputtering 20 nm of Ni onto the back (unpolished) side of the n-InP wafer and then annealing the sample under forming gas at 400 °C for 10 min. Sputter deposition of Ni was performed in an AJA Orion sputtering system. Ohmic back contacts to p-type InP were obtained by sputtering 10 nm of Zn and then 90 nm of Au onto the back side of the wafer and then annealing the sample under forming gas at 400 °C for 10 min.[2]

Epoxy-encapsulated electrodes

For electrochemical measurements made outside the glovebox, the back contact to the InP sample was attached to a coiled, tin-plated Cu wire (McMaster-Carr) using high-purity Ag paint (SPI supplies). The Cu wire was then threaded through a piece of glass tubing (Corning Incorporated, Pyrex tubing, 7740 glass). The sample was encapsulated in, and sealed to, the glass tube using Hysol 9460 epoxy, which was allowed to dry overnight under ambient conditions. The exposed areas of each electrode were imaged using a high-resolution optical scanner (Epson Perfection V370 with a resolution of 1200 psi) and the geometric areas of the electrodes (typically 0.03-0.10 cm^2) were analyzed using ImageJ software.

InP etching

Prior to electrochemical measurements, n-InP and p-InP electrodes were etched in 0.04% (by volume) Br_2/CH_3OH for 30 s, then in 4.0 M NH_3/CH_3OH for 30 s, and then rinsed in pure CH_3OH for 10 s.[3] The etching and rinsing cycle was then repeated two more times. The electrodes were blown dry for >10 s under a stream of flowing $N_2(g)$. Etching was performed outside the glove box.

Electrochemical measurements in an O_2-free environment

Electrochemical measurements on samples that were analyzed by XPS were performed in a nitrogen-filled glovebox (VAC, OMNI-LAB) using electrolytes that had been degassed in a Schlenk line (Figure S2a). The concentration of O_2 in the glove box was < 1.0 ppm as monitored by an O_2-sensitive electrode (Fuel Cell Sensor, AMI Acetic, Type T2).

To facilitate XPS analysis of the samples, electrochemical measurements were performed using a custom compression cell fabricated from PEEK (Figure S1).[4] The cell had two compartments separated by an ion-exchange membrane (Nafion for measurements in H_2SO_4, and Fumasep for measurements in KOH). Electrochemical measurements were performed using a SP-200 potentiostat (BioLogic Science Instruments) and a three-electrode set-up with either a Pt foil (for H_2SO_4) or a Ni foil (for KOH) as the counter electrode, and either a leakless miniature AgCl/Ag electrode (eDAQ, ET072-1) or a hydrogen electrode HydroFlex (Gaskatel) as the reference electrode. Electrochemical data were acquired without compensation for the series resistance of the solution. During electrochemical experiments, $H_2(g)$ was fed into the glovebox, passed through a gas bubbler, and fed

into the catholyte to constantly purge the solution (Figure S2b). Separate outlets were provided for H_2 from the cathode chamber and for O_2 from the anode chamber. Prior to each experiment, the electrochemical cell was assembled immediately after InP etching, and the assembled cell was then promptly transferred into the glovebox.

Electrochemical data were acquired on an SP-200 potentiostat (BioLogic Science Instruments) without compensation for the series resistance of the solution. To periodically measure the *J-E* behavior of illuminated p-InP/Pt electrodes, chronoamperometry (CA) was first interrupted by a short period (15 s) of open circuit to measure E_{oc}. In each cycle, cyclic voltammetry (CV) was started from $E_{start} = E_{oc}$-30 mV to < 0 V vs RHE and then ended at $E_{end} = E_{oc}$-80 mV, to minimize passing anodic current through the electrodes. Three CVs were measured during each cycle.

The main goal of this study is to elucidate the underlying corrosion pathways of p-InP photocathodes, by correlating the electrode dissolution and surface changes with the evolution of the J-E behaviors as a function of time. The total periods of the CA testing were determined based on when the J-E behavior of the electrodes stopped changing over time. Thus, the elapsed times used for the stability experiments do not reflect the ultimate limits in stability for p-InP/Pt electrodes.

In this work, evaluation of the stability of etched p-InP and p-InP/Pt photocathodes was primarily performed at E=0 V vs. RHE, to allow comparison with analogous studies in other systems.[5–7] Due to the presence of a photovoltage, applying this E produces substantial cathodic current density at start of the CA, as expected based on the position of the maximum power point in an efficient PEC system. The cathodic current density also determines the surface quasi-Fermi level position of minority carriers, as well as the corrosion pathways of InP in the Pourbaix diagram. Thus, our further evaluation of surface chemistry was performed at this specific E. Similarly for n-InP electrodes, E=-0.1 V vs. RHE was chosen to match the quasi-Fermi level position of majority carriers with the overpotential of Pt HER catalyst.

A miniature fiber-optic adjustable-arm light equipped with a 150 W halogen bulb was used as the illumination source. Illumination was introduced from the source into the glove box via the fiber optic. The illumination intensity at the location of the sample in the cell was calibrated to 1 Sun (100 mW cm^{-2}) using a Si photodiode (FDS100, Thorlabs). The volume of electrolyte in the cathode

chamber was 3-4 mL. For each ICP-MS analysis, 0.2 mL of electrolyte was removed from the cell at different time intervals and 0.2 mL of fresh electrolyte was added into the cell. After each experiment was completed, the cell was disassembled inside the glove box, and the electrode sample was thoroughly cleaned with deionized water, dried under stream of flowing N_2(g), and stored inside the glove box until the surface was analyzed by XPS.

Figure S32 compares the corrosion thickness of n-InP electrodes (dark) held at E=-0.1 V vs. RHE in H_2-saturated and O_2-saturated 1.0 KOH electrolytes. However, the underlying corrosion mechanism of InP induced by oxygen exposure is the topic of a separate study but is not relevant to an operating photocathode in which the catholyte should be maintained under 1 atm of H_2 to obtain intrinsically safe operation as well as to minimize efficiency losses due to reduction of O_2 in competition with the HER.

Electrodeposition of Pt particles

A solution of 5 mM K_4PtCl_6 and 0.5 M KCl was used to electrodeposit Pt particles onto InP samples. A constant current density of -0.2 mA cm^{-2} was applied using a two-electrode configuration until 20 mC cm^{-2} had passed. Before each deposition, bubbles accumulating in the electrode area were carefully removed to ensure the uniformity of electrodeposition. The deposition was performed under ~1 Sun illumination for p-InP and in the dark for n-InP. Either a Pt wire or a carbon rod was used as the counter electrode for the deposition. The cell was then thoroughly cleaned with deionized water at least 3 times before the 1.0 M H_2SO_4 or 1.0 M KOH electrolyte used for electrochemical experiments was added to the cell. For the stability test of p-InP/Pt in 1.0 M KOH(aq), the Pt deposition and the subsequent hydrogen-evolution reaction (HER) process were performed in two separate cells to minimize cross-contamination.

Electrochemistry outside glovebox

A series of chronoamperometry (CA) and cyclic voltammetry (CV) experiments for n-InP (dark) and p-InP (light) were performed in a two-compartment cell outside the glove box under a continuous H_2 purge (Figure S2). These experiments did not involve XPS analyses after electrochemical operation. The CA experiments were performed by potentiostatically holding freshly etched InP electrodes at

specified potentials for 30 min. At least three voltammetric cycles were then scanned in the positive direction from the original polarization potential to potentials sufficient to oxidize any deposited In metal.

Electrochemical measurements were performed using a custom two-compartment electrochemical cell with a Nafion (1.0 M H_2SO_4) or Fumasep (1.0 M KOH) membrane separating the two compartments. The electrochemical cell was cleaned with aqua regia before use. The volume of the electrolyte used in the cathode compartment was 20 or 25 mL. A mercury/mercurous sulfate ($Hg/HgSO_4$ in saturated K_2SO_4(aq), CH Instruments, CH151) reference electrode was used for measurements in 1.0 M H_2SO_4(aq). A mercury/mercury oxide (Hg/HgO in 1.0 M KOH (aq), CH Instruments, CH152) reference electrode was used for measurements in 1.0 M KOH (aq). A carbon rod placed within a fritted glass tube (gas dispersion tube Pro-D, Aceglass, Inc.) was used as the counter electrode. Both the $Hg/HgSO_4$ and the Hg/HgO reference electrodes were calibrated versus a reversible hydrogen electrode (RHE). The Hg/HgO electrode potential was 0.910 V versus RHE in 1.0 M KOH (aq). The $Hg/HgSO_4$ electrode potential was 0.683 V versus RHE in 1.0 M H_2SO_4 (aq).

Electrochemical data were acquired on an MPG-2 multichannel potentiostat (BioLogic Science Instruments) without compensation for the series resistance of the solution. During measurements, the electrolyte was continually bubbled with 1 atm of H_2(g) and vigorously agitated with a magnetic stir bar driven by a model-train motor (Pittman) with a Railpower 1370 speed controller (Model Rectifier Corporation) or a magnetic stirrer (IKA Topolino). 50 W ENH-type (Philips MR16) W-halogen lamps with dichroic rear reflectors and custom housings and transformers (Staco Energy Products Co.) were used for photoelectrochemical measurements. The illumination intensity at the position of the working electrode in the electrochemical cell was determined by placing a calibrated Si photodiode (FDS100-Cal, Thor Labs) into the cell at the same position occupied by the photoelectrode. To illuminate the bottom-facing photoelectrodes, a broadband reflection mirror (Newport dielectric mirror) was used to direct the uniform light beam in the vertical direction.

Mott-Schottky Analyses

Impedance measurements of freshly etched n-InP and p-InP electrodes, in contact with 1.0 M H_2SO_4(aq) or 1.0 M KOH(aq) under H_2(g) bubbling, were collected in the dark over a frequency

range of 20 Hz to 20 kHz with a sinusoidal wave amplitude of 25 mV. The measurements were performed outside the glove box. The impedance measurements were fit with a circuit consisting of a resistor in series with an additional component consisting of a resistor and a capacitor in parallel.[8,9] The potential dependence of the differential capacitance was analyzed using the Mott-Schottky relationship:

$$C_d^{-2} = \frac{2}{qA^2\varepsilon_0\varepsilon_r N_d}(V_{app} + V_{bi} - \frac{k_B T}{q})$$

where C_d is the differential capacitance, q is the unsigned charge of an electron, A is the electrode area, ε_0 is the vacuum permittivity, ε_r is the relative permittivity of the semiconductor, N_d is the dopant concentration of the semiconductor, V_{app} is the applied electrode potential, V_{bi} is the built-in voltage in the semiconductor, and T is the temperature of the electrode while the impedance data were collected. A relative permittivity of $\varepsilon_r = 8.8$ was used to analyze data for InP electrodes.

Analytical Methods

Inductively coupled plasma mass spectrometry (ICP-MS)

Inductively coupled plasma mass spectrometry (ICP-MS) data were collected using an Agilent 8800 Triple Quadrupole ICP-MS system. Calibration solutions were prepared by diluting the multi-element standard solutions for ICP with water having a resistivity of 18.2 MΩ cm. All electrolyte samples were acidified to pH ≤2 before the ICP-MS measurements. The total amounts of In dissolved from the electrodes were calculated and normalized to the geometric electrode area to yield the equivalent depth of material removed from the InP electrode. The error bars of each data point represent the standard deviations of five consecutive measurements using the instrument. Due to the high detection limit of phosphorus (P) by ICP-MS, only the concentrations of In ions were used to calculate the corrosion thickness of InP. The conversion equation relating the In concentration (ug/L) as measured by ICP-MS to the dissolution thickness of InP (nm) is shown below:

$$InP\ Thickness\ (nm) = \frac{x\ \mu g}{1\ L}(In\ concentration) * \frac{3.2\ mL}{0.2\ mL}(dilution\ factor) * 4\ mL(total\ volumer\ of\ ca$$
$$* \frac{1\ L}{1000\ mL} * \frac{1 * 10^{-6}\ g}{1\ \mu g} * \frac{1\ mol}{114.8\ g}(In\ molar\ mass) * \frac{(114.8 + 31)\ g}{1\ mol}$$
$$(InP\ molar\ mass) * \frac{1\ cm^3}{4.81\ g}(InP\ density) * \frac{1}{0.2\ cm^2}(electrode\ area) * \frac{1 * 10^7\ nm}{1\ cm}$$

The dilution factor, the total volume of catholyte and the electrode area shown above are typical values which are specific to each experiment.

X-ray photoelectron spectroscopy

X-ray photoelectron spectroscopy (XPS) was performed using a Kratos Axis Ultra system with a base pressure of < 1×10^{-9} Torr equipped with a monochromatic Al Kα X-ray source with a photon energy of 1486.6 eV. Photoelectrons were collected at 0° from the surface normal with a retarding pass energy of 160 eV for survey XPS scans (step sizes of 1.0 eV and 10 eV) and for high-resolution core-level scans (step size 0.025 eV).

Prior to XPS measurements, samples were mounted on a sample holder and loaded in a transfer box inside the glove box under nitrogen. The transfer box was attached to the load lock of the Kratos Axis Ultra system with the transfer box gate valve (VAT) still closed (Figure S2c). The load lock was first pumped down and purged again with N_2. After pumping down the load lock again to 1×10^{-2} Torr, the gate valve to the transfer box was opened and the turbo molecular pump was switched on. After achieving a pressure of <1 x 10^{-6} Torr, the sample was transferred to the sample-transfer chamber (base pressure <1×10^{-9} Torr) before further transfer to the analysis chamber.

All XPS peak fitting was performed using CasaXPS software version 2.3.18. All binding energies are referenced to the adventitious carbon peak at 284.8 eV. Before fitting the data, a Shirley background was calculated and subtracted from the original spectra. The major peak of the In^{3+} cations of InP in the In 3d spectra was fit using an asymmetric Lorentzian function LF(1,1,15,80). All other peaks were fit using the 70% Gaussian/30% Lorentzian Voigt-function. The surface In/P atomic ratios were calculated using the relative sensitive factors (RSF) in the database of the Kratos instrument and the peak areas (In=7.265, P=0.486). In addition, the criteria of XPS peak assignments

to various In-containing species including InP, InO_x, $In(OH)_x$ and $InPO_x$ is shown in Table S4.[10–22] We also collected XPS data of various control samples (InP with native oxide, ITO and In foils) on the same instrument to further support the XPS peak assignment, which are shown in Figure S33-35.

In this work, we used single-crystal p-InP(100) electrodes with thicknesses of 625 μm. However, electrochemical experiments using either etched p-InP or p-InP/Pt electrodes only revealed surface changes over the range of a few nm. Due to its relatively large penetration depth, XRD analyses of both etched p-InP and p-InP/Pt electrodes before and after CA will likely yield similar patterns with major features assigned to the lattice of crystalline InP. In contrast, the high surface sensitivity and relatively low photoelectron escape depth of XPS provides a more direct probe of changes in the surface and consequently facilitates determination of the corrosion pathways. In addition, the dipole energy formed at the InP/electrolyte interface shown in Scheme 1 is not measurable by ultraviolet photoelectron spectroscopy (UPS) under ultrahigh-vacuum conditions.

Microscopy

Scanning-electron microscopy (SEM) images were obtained using a calibrated Nova NanoSEM 450 (FEI) with an accelerating voltage of 5 kV.

Transmission-electron microscopy (TEM) cross-sections of the samples were prepared using a focused Ga ion beam (FIB), on a FEI Nova-600 Nanolab FIB/FESEM or a FEI Helios NanoLab G4 Dual Beam. Pt and C protection layers were applied prior to exposure to the FIB. TEM images of the prepared lamella samples were obtained using a Tecnai Polara (F30) TEM at an accelerating voltage of 300 kV, or a FEI Osiris at an accelerating voltage of 200 kV equipped with a Gatan 2K TEM camera and Bruker EDS.

Atomic-force microscopy (AFM) images were obtained on a Bruker Dimension Icon using Bruker ScanAsyst-Air probes (silicon tip, silicon nitride cantilever, spring constant: 0.4 N m^{-1}, frequency: 50-90 kHz), operating in the ScanAsyst mode. Images were analyzed using the Nanoscope Analysis software (version 1.9).

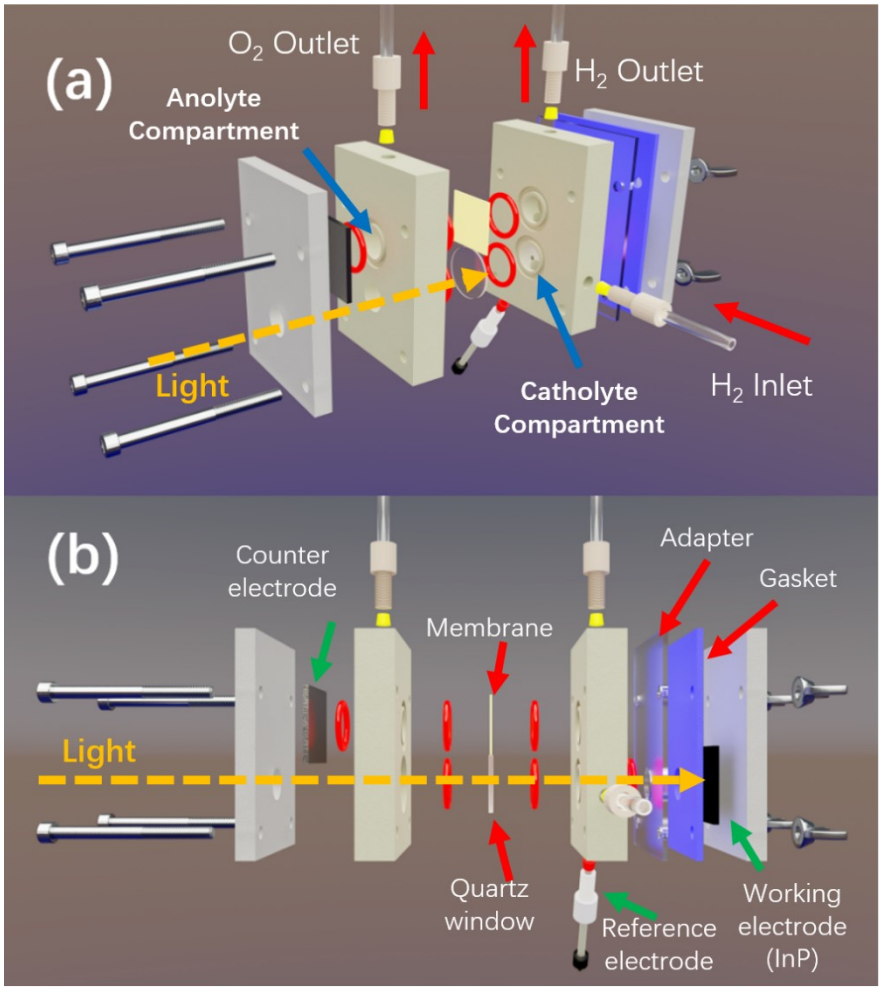

Figure S1. (a,b) Two views of the design of the photoelectrochemical compression cell used for electrochemical measurements in an O_2-free environment. The current collector (Al foil) at the back of both working and counter electrode are omitted for simplicity. Before each experiment, electrolyte was added through the ports of H_2 and O_2 outlets before the respective tubes were connected. During each experiment, the electrolyte in the catholyte compartment was sampled (0.2 mL) through the H_2-outlet port after disconnecting the tube, while the working electrode was still under potential control.

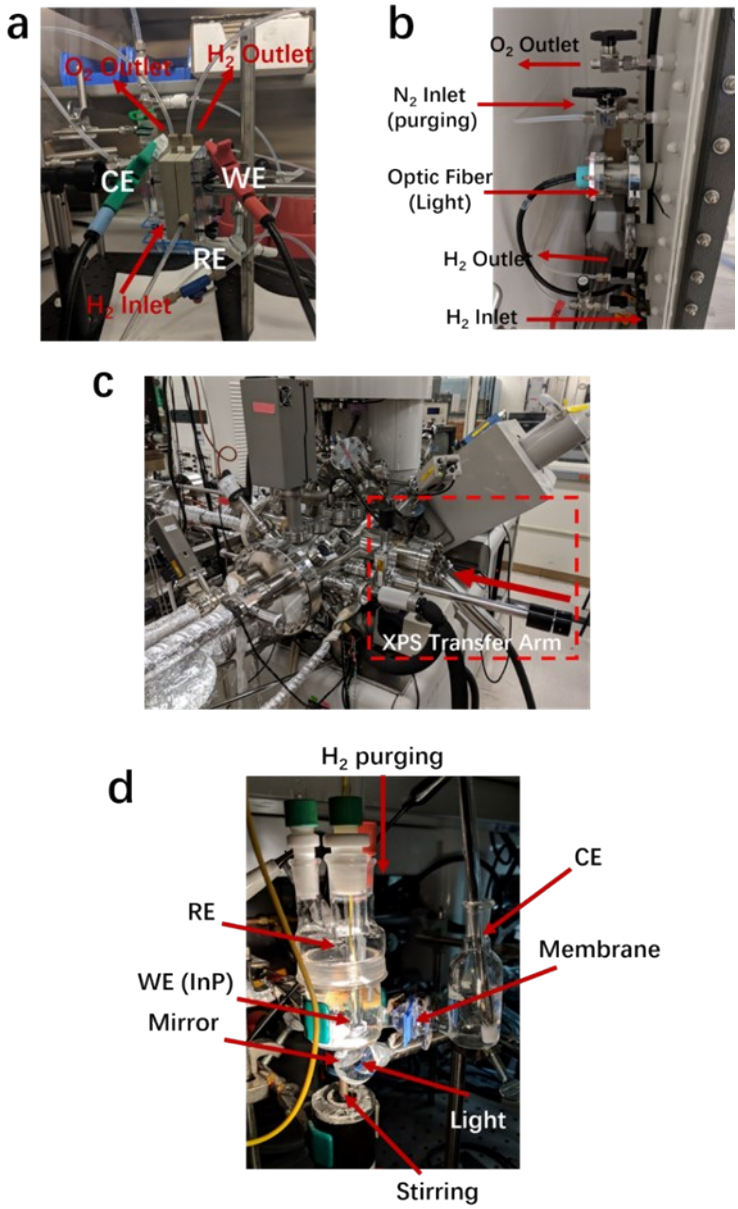

Figure S2. Experimental setup. (a) The custom cell illustrated in Figure S1 being tested inside a N_2-filled glovebox. (b) Modifications to the glove box to allow experiments to be performed with H_2 purging, light illumination and post-test N_2 purging. (c) The air-free transfer arm attached to the XPS instrument. After the EC cell was disassembled, the sample was rinsed with deionized water, purged with N_2, and loaded onto the transfer arm inside the glove box. The transfer arm was transferred from the glove box to the XPS. (d) A two-compartment cell used for testing outside the glove box while purging with H_2.

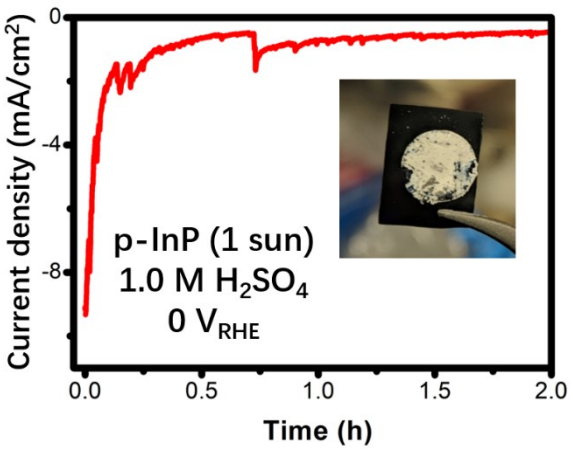

Figure S3. (a) Chronoamperometry (CA) for 2 h at 0 V vs RHE in 1.0 M H_2SO_4(aq) of an illuminated etched p-InP electrode. The inset shows the p-InP electrode after the CA; the whitish area was inside the O-ring and exposed to the electrolyte.

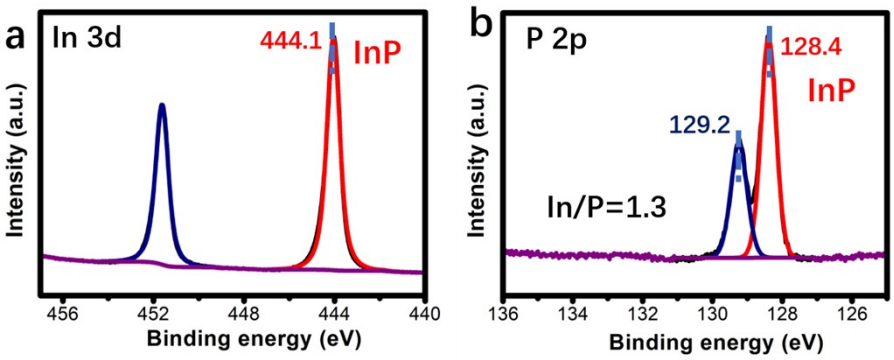

Figure S4. XPS data of (a) In 3d and (b) P 2p regions of a p-InP sample without exposure to electrolyte.

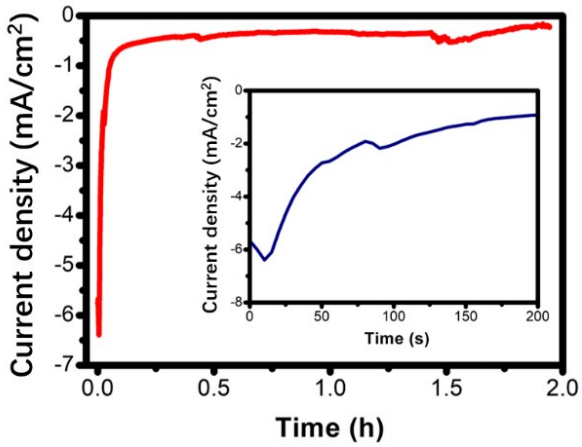

Figure S5. (a) Chronoamperometry (CA) of an illuminated etched p-InP electrode for 2 h at -0.2 V vs RHE in 1.0 M KOH(aq). The inset shows the data for the first 200 s.

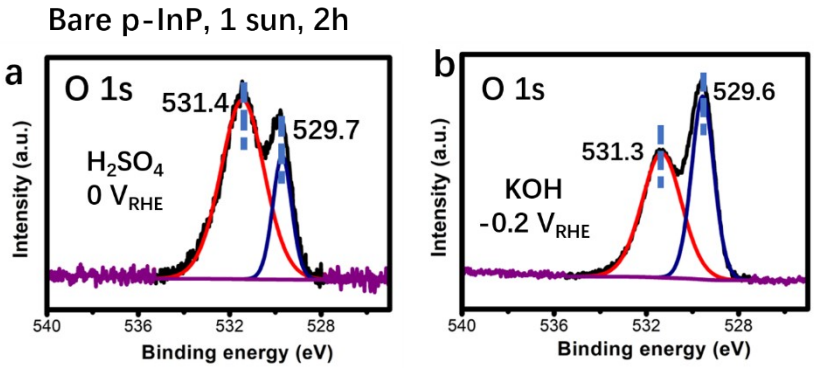

Figure S6. Comparison of XPS data for the O 1s region of an illuminated etched p-InP electrode (1 sun) tested (a) for 2 h at 0 V vs RHE in 1.0 M H_2SO_4(aq) and (b) for 2 h at -0.2 V vs RHE in 1.0 M KOH(aq).

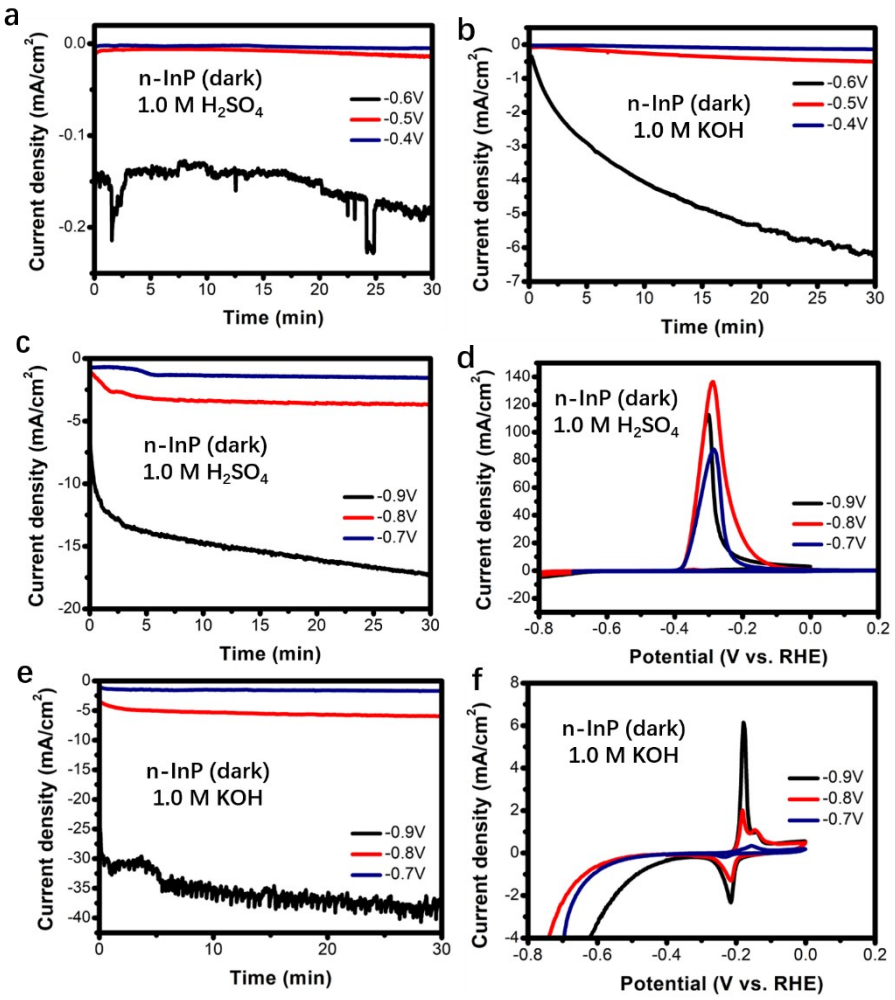

Figure S7. (a-c,e) Chronoamperometry of n-InP electrodes held at various potentials, *E* (from -0.4 to -0.9 V vs RHE) in the dark, while in contact with (a,c) 1.0 M H_2SO_4(aq) and (b,e) 1.0 M KOH(aq). (d,f) Comparison of CVs performed after the CAs shown in (c,e), scanning in a positive direction from the initially applied *E* (scan rate: 20 mV s^{-1}).

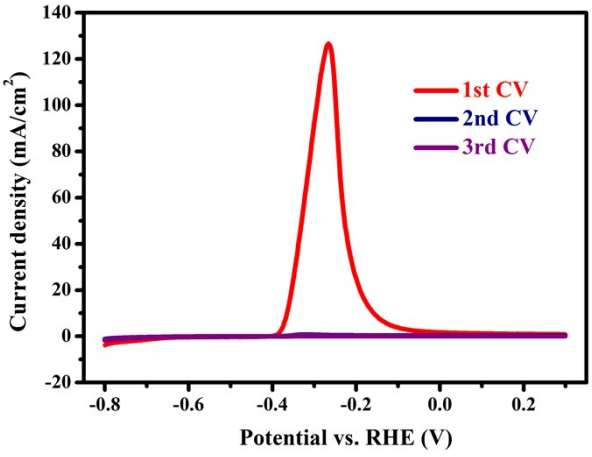

Figure S8. Three consecutive CVs collected for an n-InP electrode after the electrode was held for 30 min at -0.8 V vs RHE in 1.0 M H_2SO_4(aq) in the dark. Scan rate: 20 mV s^{-1}.

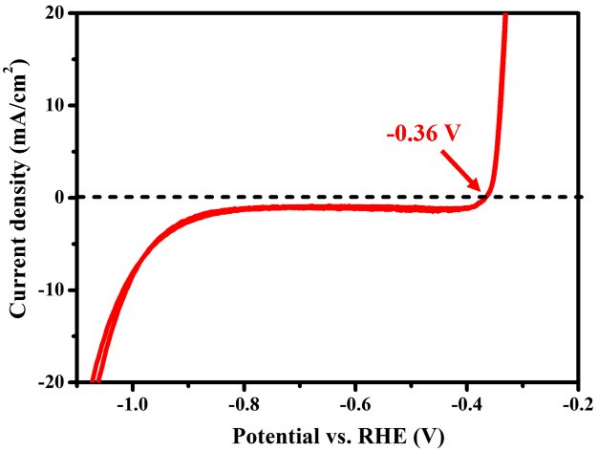

Figure S9. CV of an In metal foil electrode in 1.0 M H_2SO_4(aq). The onset potential for anodic current was -0.36 V vs RHE. Scan rate: 20 mV s^{-1}.

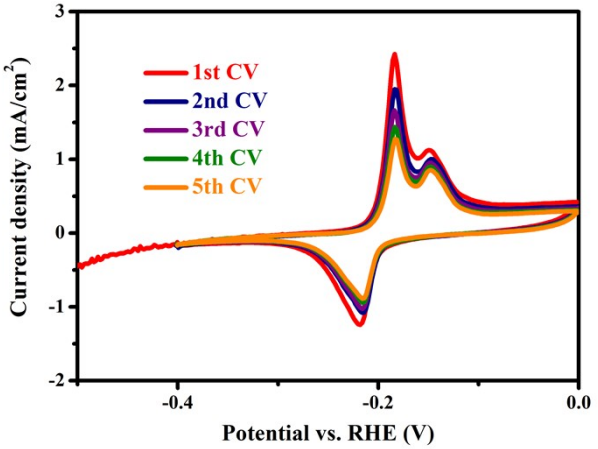

Figure S10. Five consecutive CVs collected for an n-InP electrode for 30 min at E=-0.8 V vs. RHE in 1.0 M KOH(aq) in the dark. Scan rate is 20 mV s^{-1}.

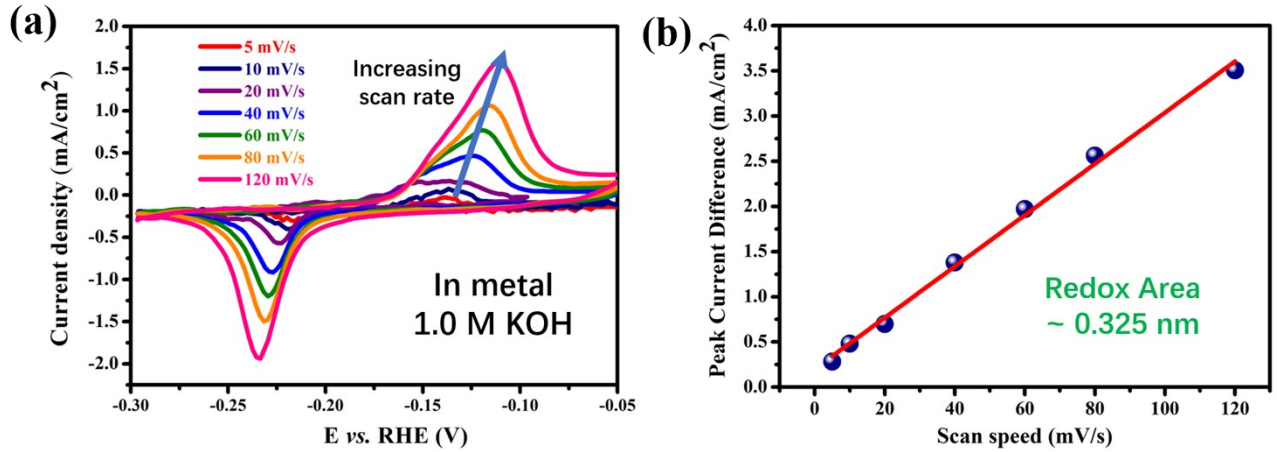

Figure S11. (a) Scan-rate dependence of CVs of an In metal foil electrode in contact with 1.0 M KOH(aq). (b) Dependence of the differences between the anodic and cathodic peaks in J as a function of scan rate. The thickness of the redox-active layer on the electrode was calculated as 0.33 nm.

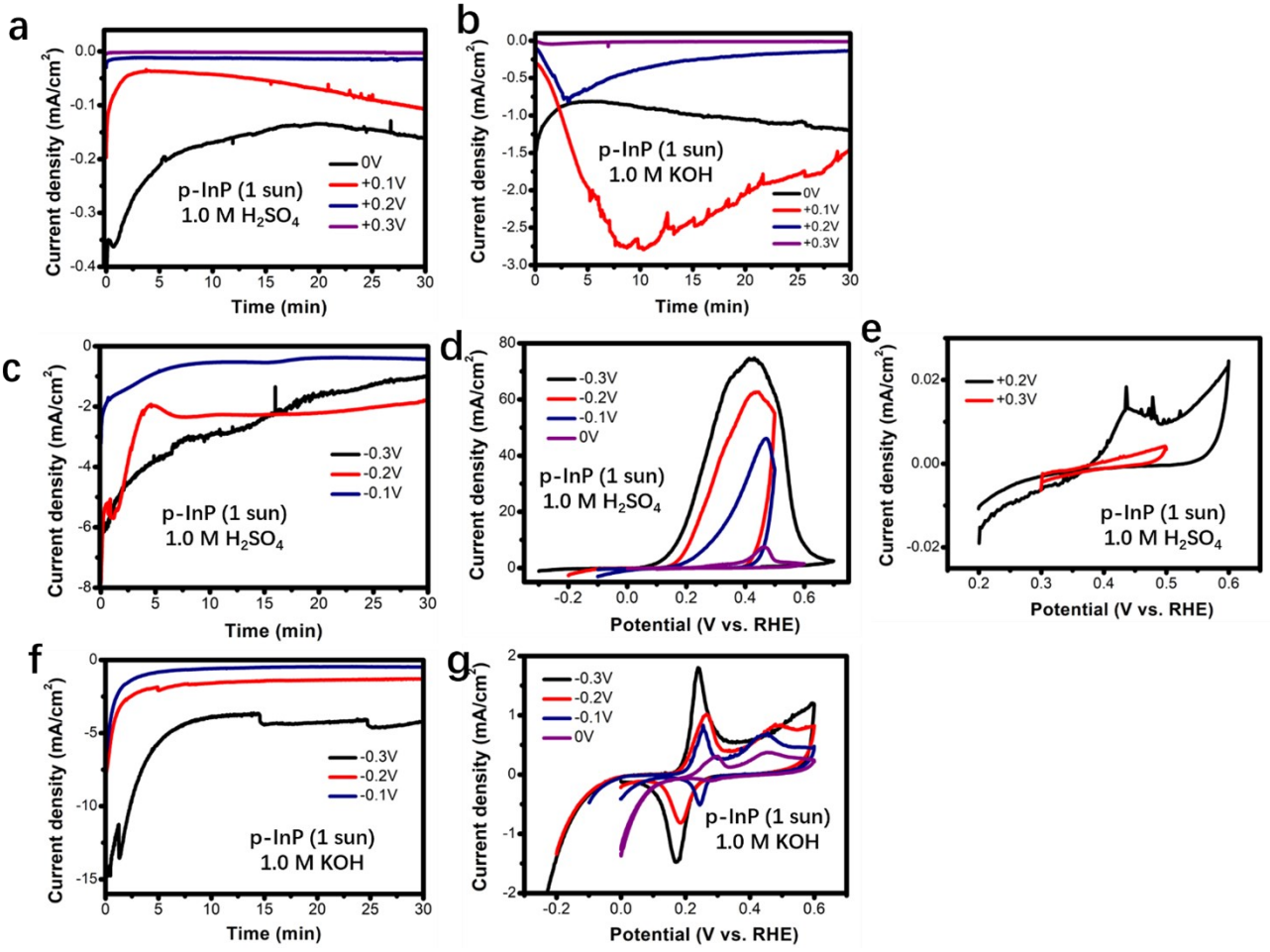

Figure S12. (a-b) Chronoamperometry of illuminated p-InP electrodes held for 30 min between 0 and +0.3 V vs. RHE in (a) 1.0 M H_2SO_4(aq) and (b) 1.0 M KOH(aq). (c,f) Chronoamperometry of illuminated p-InP electrodes held for 30 min at between -0.3 and 0 V vs RHE in (c) 1.0 M H_2SO_4(aq) and (f) 1.0 M KOH(aq). (d,e,g) CVs performed after the experiment shown in (c,f), scanning in a positive direction from the initially applied potential using a scan rate of 20 mV s^{-1}. The illumination intensity was 100 mW cm^{-2} (1 sun).

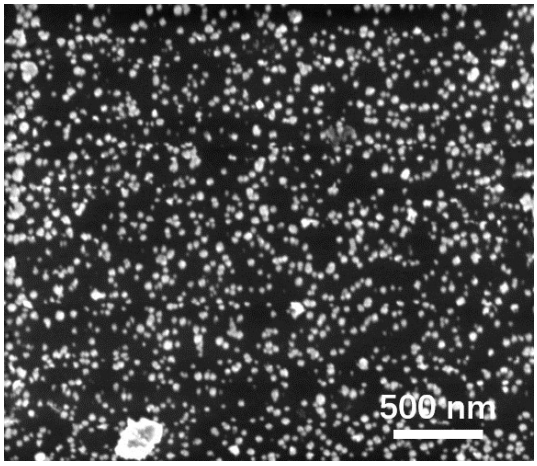

Figure S13. SEM image of the surface morphology of an as-prepared p-InP/Pt electrode

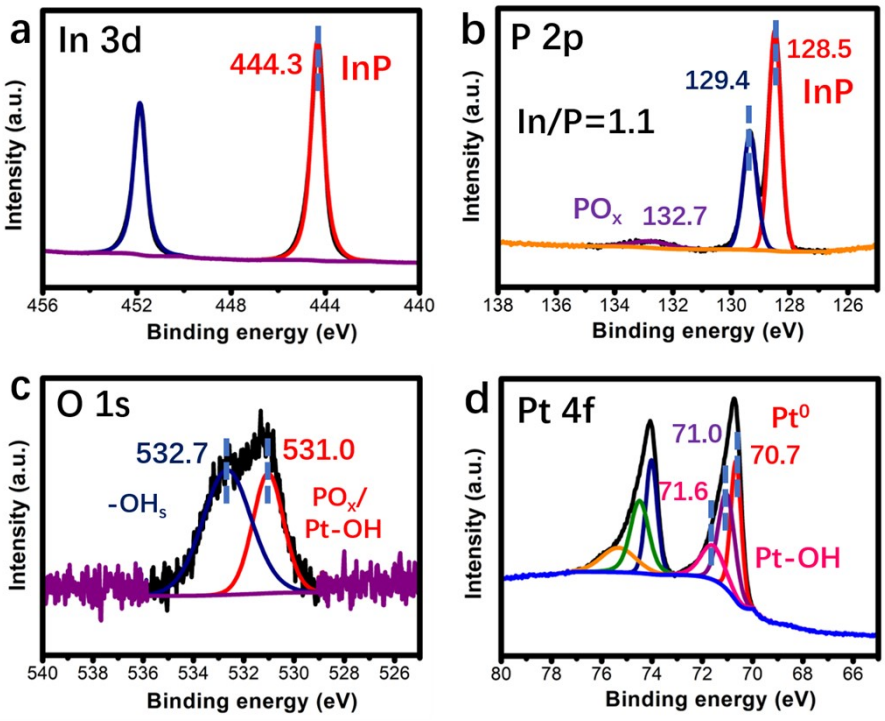

Figure S14. XPS data of (a) In 3d, (b) P 2p, (c) O 1s and (d) Pt 4f regions for an as-prepared p-InP/Pt electrode before CA.

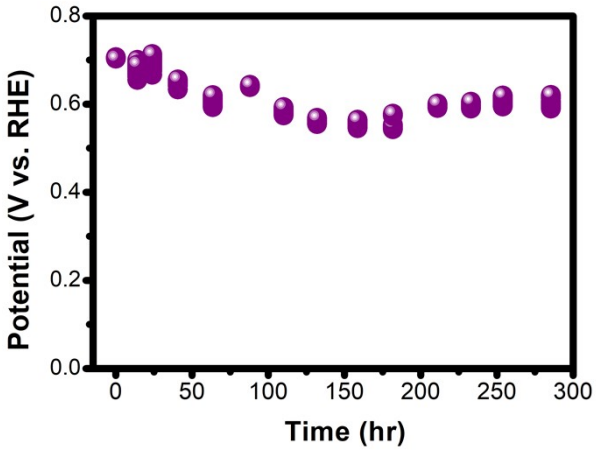

Figure S15. E_{oc} versus time periodically measured for a p-InP/Pt electrode tested for 285 h at 0 V vs RHE in 1.0 M H_2SO_4(aq) under 1-sun illumination.

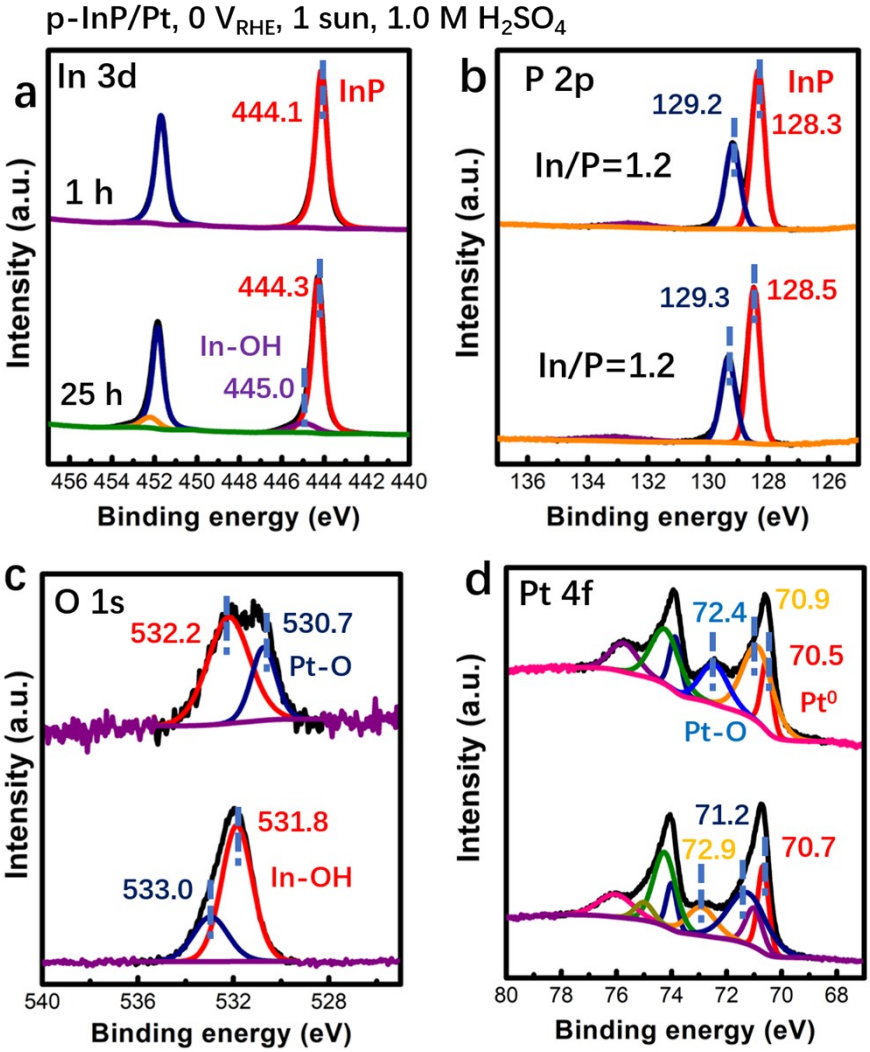

Figure S16. XPS data of (a) In 3d, (b) P 2p, (c) O 1s and (d) Pt 4f regions for illuminated p-InP/Pt electrodes (1 sun) at 0 V vs RHE for 1 h and 25 h, respectively, in 1.0 M H_2SO_4(aq).

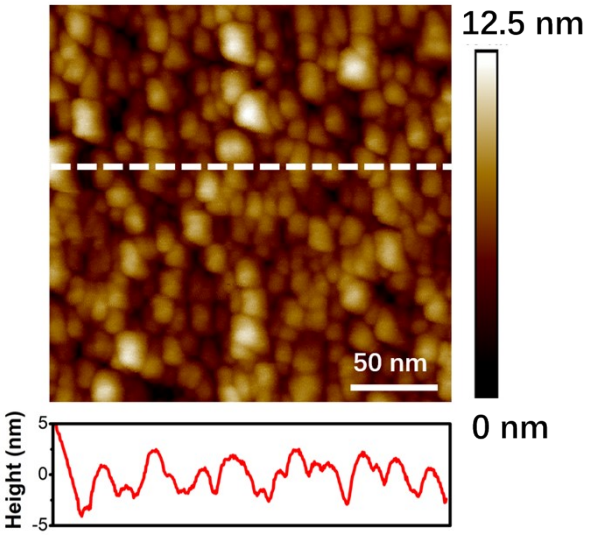

Figure S17. AFM image of the flat region of an illuminated p-InP/Pt electrode (1 sun) held for 72 h at 0 V vs RHE in 1.0 M KOH(aq).

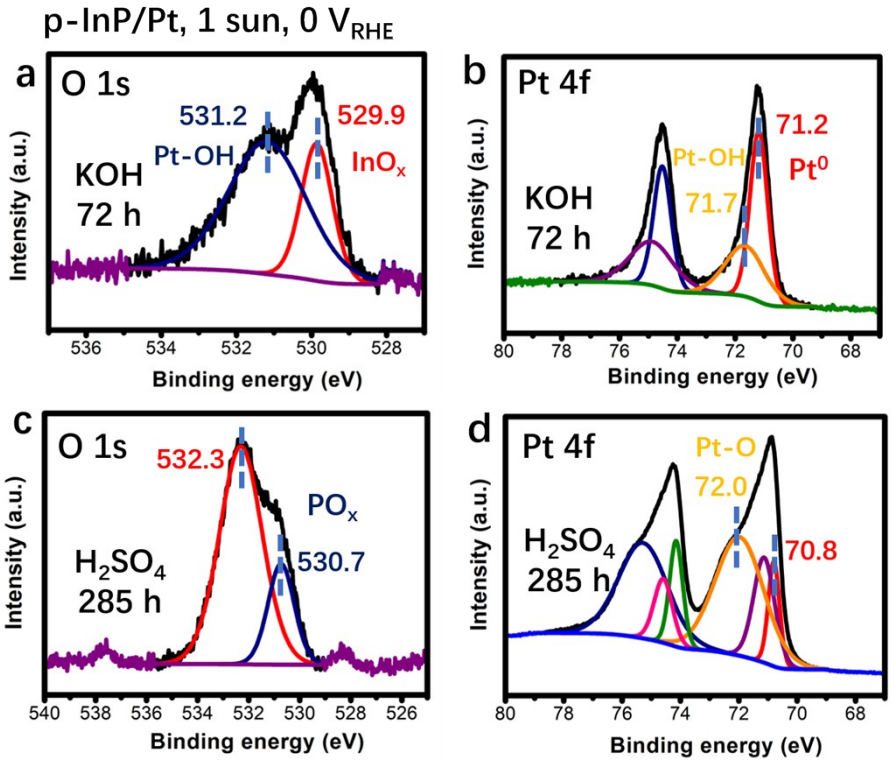

Figure S18. Comparison of the XPS data of (a,c) O 1s and (b,d) Pt 4f regions for illuminated p-InP/Pt electrodes (1 sun) tested for 72 h at 0 V vs RHE (a-b) in 1.0 M KOH(aq) and (c-d) for 285 h at 0 V vs RHE in 1.0 M H_2SO_4(aq).

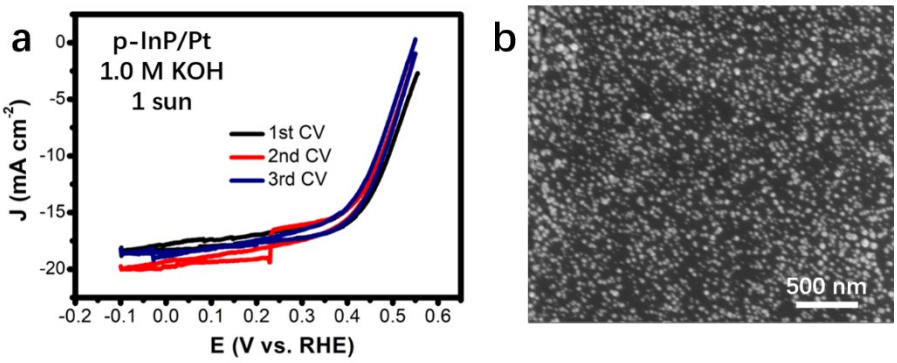

Figure S19. (a) Comparison of three consecutive CV scans of an illuminated p-InP/Pt electrode (same as Figure S16). The scan direction was from -25 mV vs. E_{oc} to -0.1 V vs RHE and the scan rate was 50 mV s^{-1}. (b) SEM image of the p-InP/Pt electrode after undergoing 3 CVs in (a).

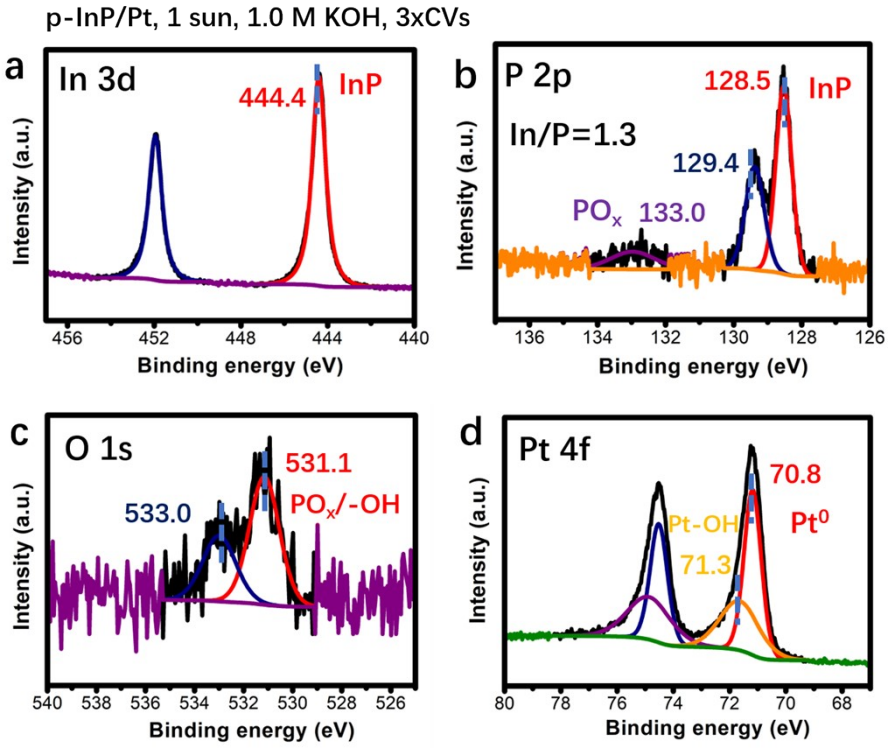

Figure S20. XPS data of (a) In 3d, (b) P 2p, (c) O 1s and (d) Pt 4f regions of a p-InP/Pt electrode after undergoing 3 cycles of CVs in 1.0 M KOH(aq) under 1-sun illumination in Figure S18.

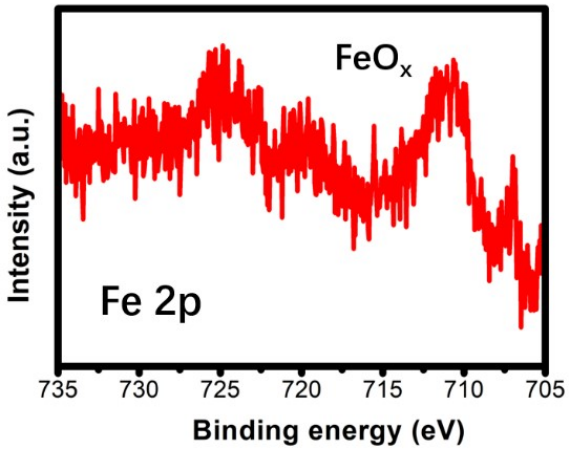

Figure S21. XPS data of the Fe 2p region of a p-InP/Pt electrode after the CA test in Figure 4, showing the presence of trace FeO_x (BE~711 eV).

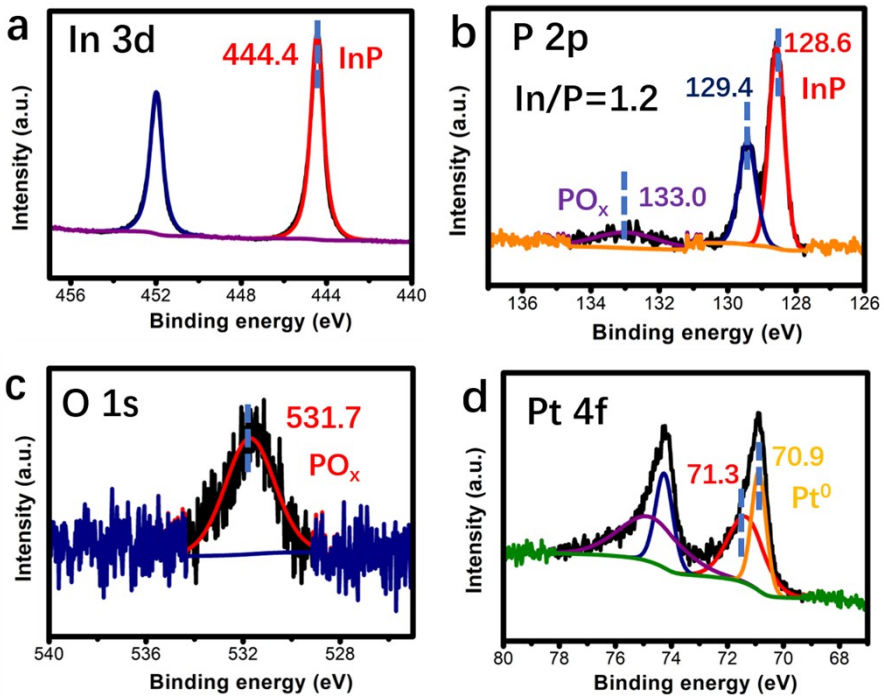

Figure S22. XP spectra of the (a) In 3d, (b) P 2p, (c) O 1s and (d) Pt 4f spectral regions of the p-InP/Pt electrode after the series of electrochemical experiments shown in Figure 6. After switching to 1.0 M H_2SO_4(aq), the p-InP/Pt electrode was first tested by CV followed by a 4-h CA at 0 V vs. RHE, before the XPS data was collected.

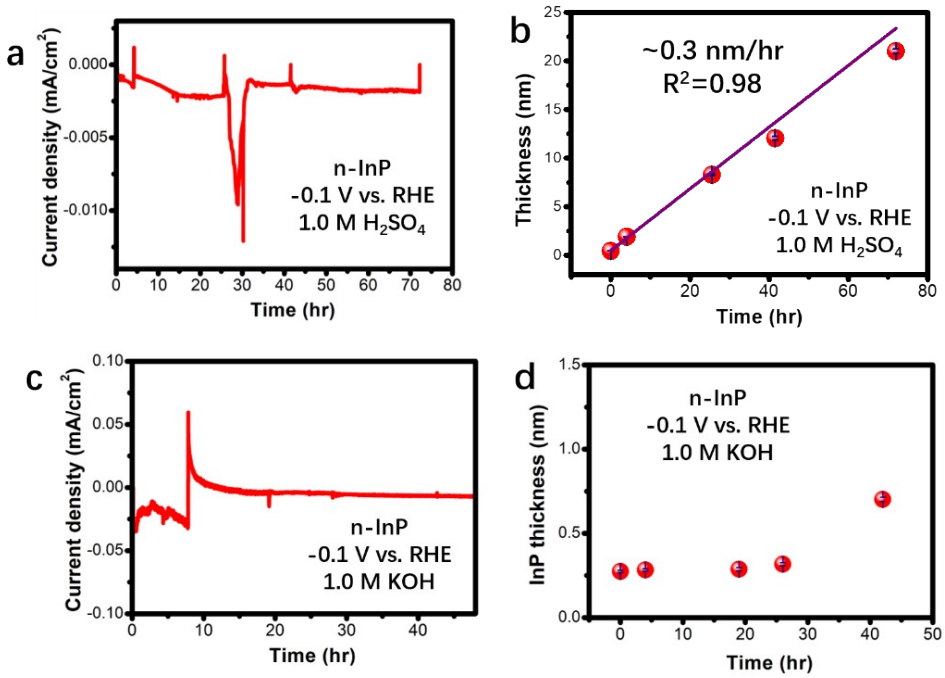

Figure S23. (a,c) Chronoamperometry of n-InP electrodes held at -0.1 V vs RHE in the dark in (a) 1.0 M H_2SO_4(aq) and (c) 1.0 M KOH(aq) and (b,d) the electrode dissolution thickness measured throughout the CA in (a,c). The n-InP electrodes displayed a linear dissolution rate of 0.3 nm h^{-1} in 1.0 M H_2SO_4(aq) but negligible dissolution in 1.0 M KOH(aq).

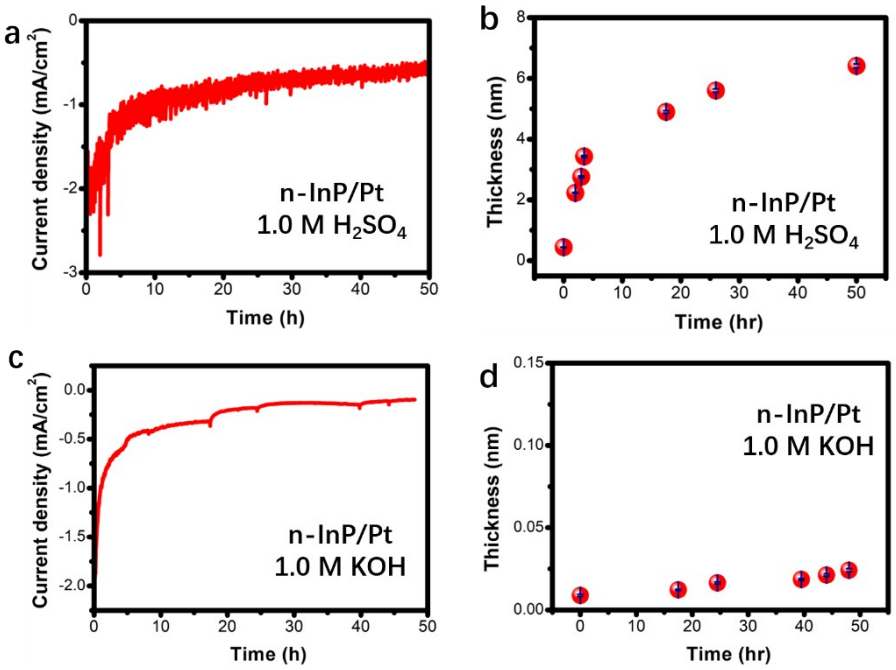

Figure S24. (a,c) Chronoamperometry of n-InP/Pt electrodes held at -0.1 V vs RHE in the dark in (a)

1.0 M H_2SO_4(aq) and (c) 1.0 M KOH(aq) and (b,d) the electrode dissolution thickness measured throughout the CA in (a,c).

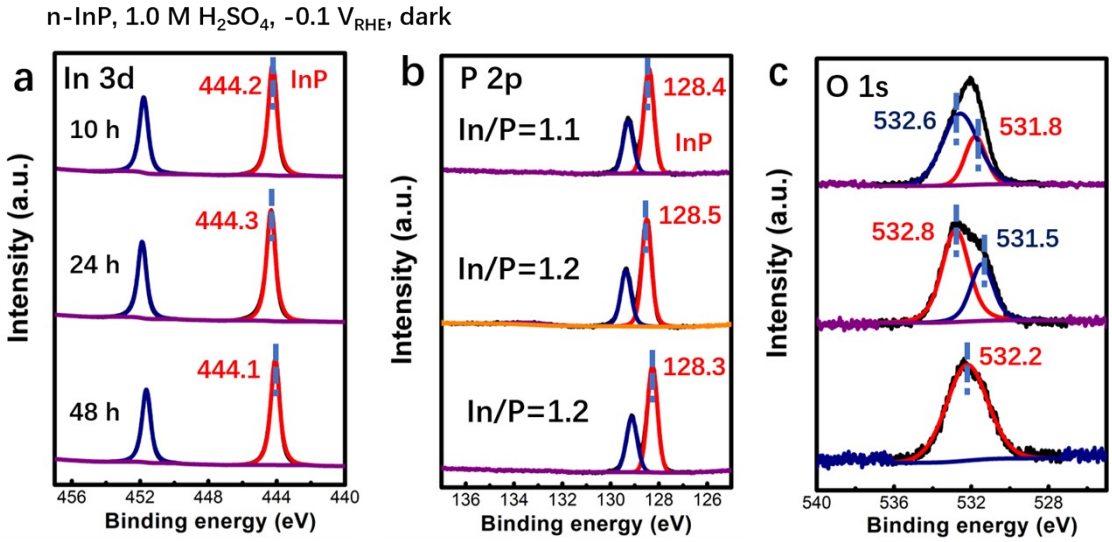

Figure S25. XPS data of the (a) In 3d, (b) P 2p and (c) O 1s regions of three different n-InP electrodes held at -0.1 V vs RHE in 1.0 M H_2SO_4(aq) for 10 h, 24 h and 48 h, respectively.

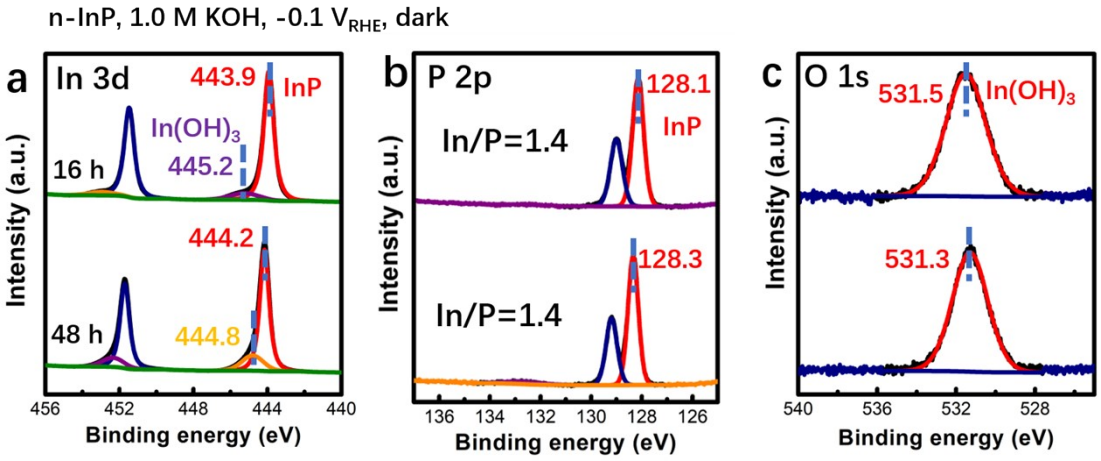

Figure S26. XPS data of the (a) In 3d, (b) P 2p and (c) O 1s regions of two different n-InP electrodes held at -0.1 V vs RHE in 1.0 M KOH(aq) for 10 h, 24 h and 48 h, respectively. The small peaks seen at high BE (444.8 or 445.2 eV) of the In 3d XPS are ascribable to the surface $In(OH)_3$ species.

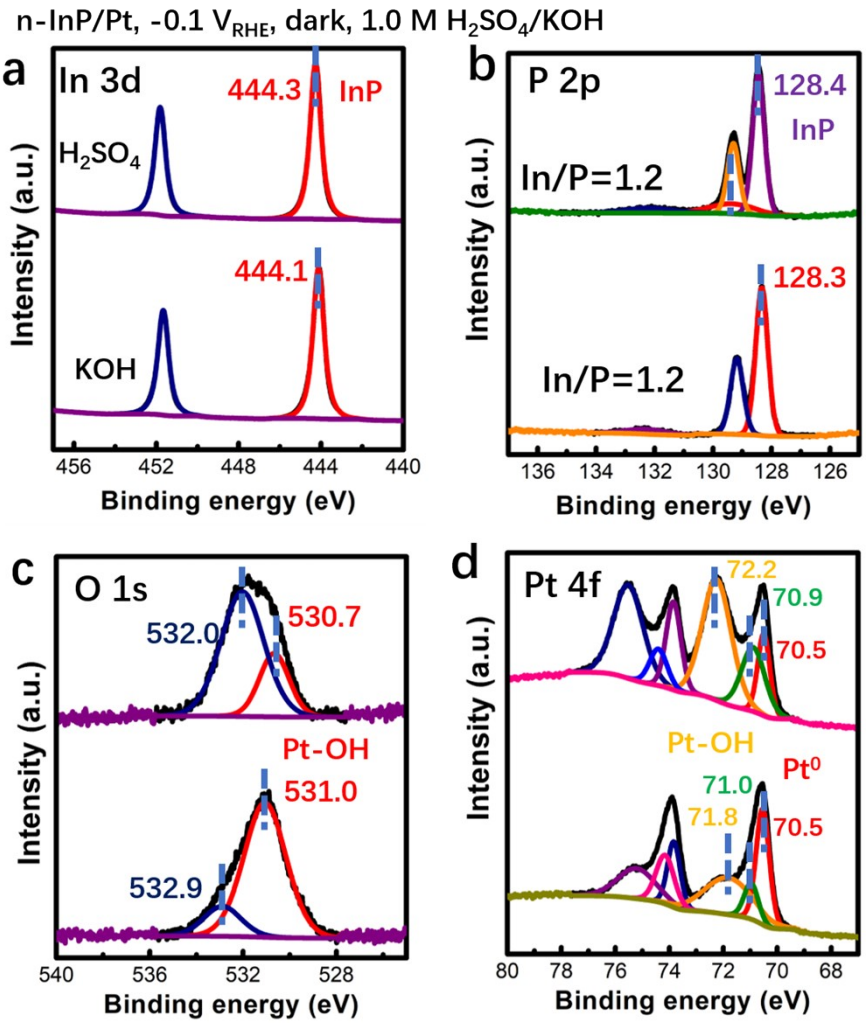

Figure S27. XPS data of the (a) In 3d, (b) P 2p, (c) O 1s and (d) Pt 4f region of n-InP/Pt electrodes held at -0.1 V vs RHE in 1.0 M H_2SO_4(aq) and 1.0 M KOH(aq) in Figure S25.

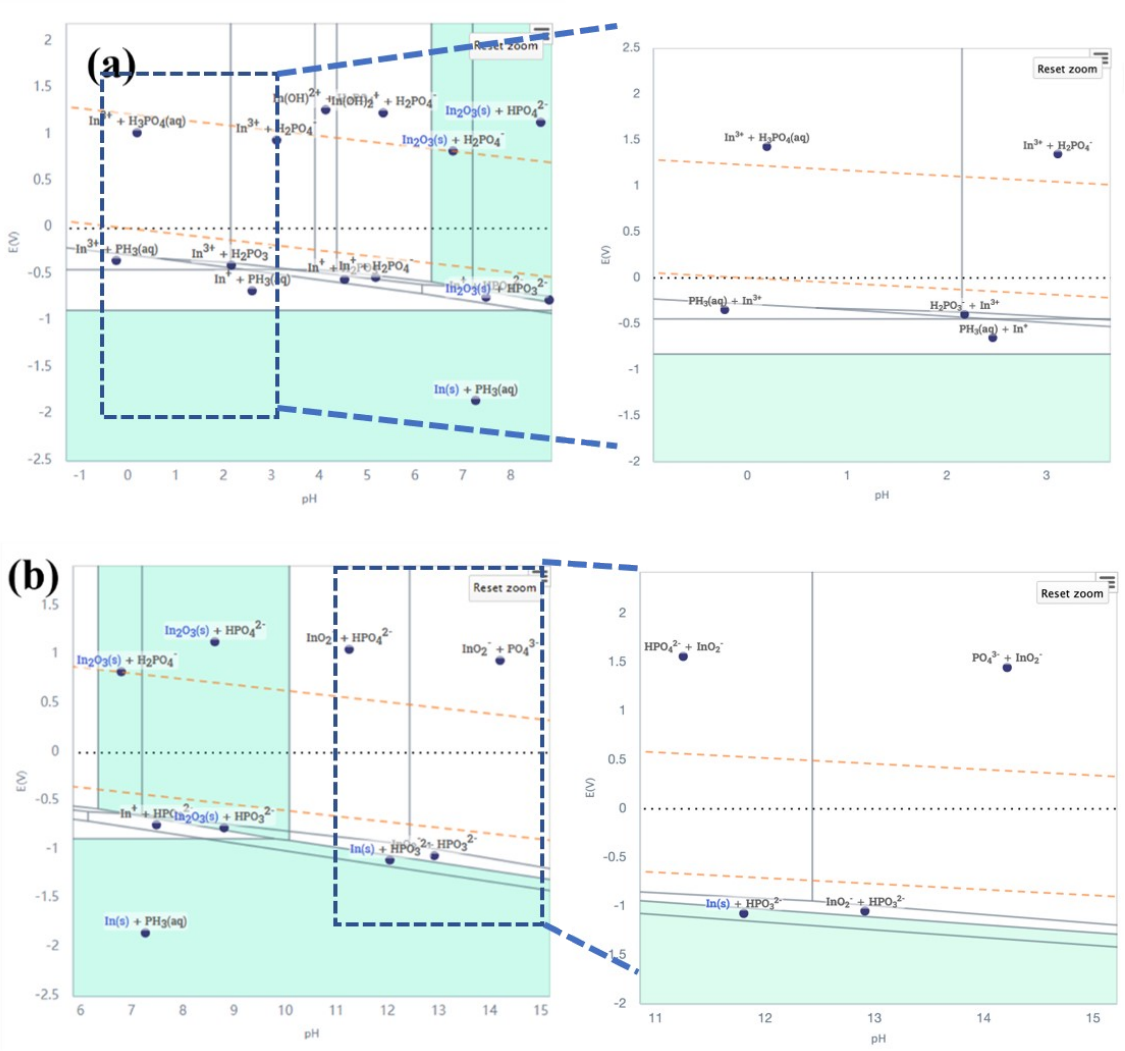

Figure S28. Calculated Pourbaix diagrams for the In-P (In/P=1) system at low concentration of $1x10^{-8}$ mol kg^{-1} in (a) acidic and (b) alkaline electrolyte, produced by the Materials Project.[23]

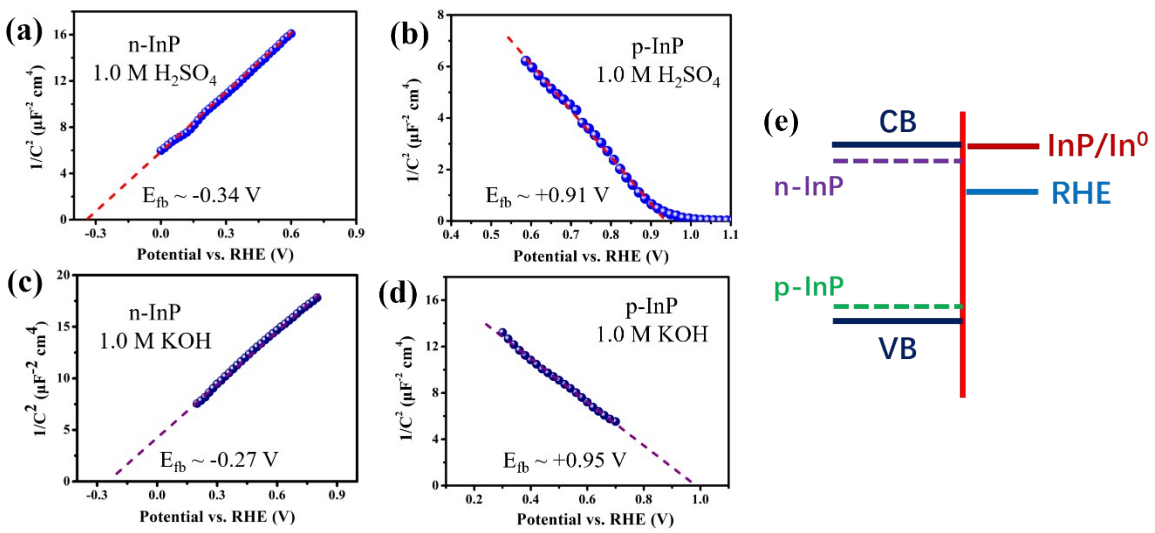

Figure S29. (a-d) Mott-Schottky analyses for (a,c) n-InP and (b,d) p-InP electrodes measured in the dark while in contact with (a,b) 1.0 M H_2SO_4(aq) and (c,d) 1.0 M KOH(aq). (e) Analysis of the interfacial energetics comparing the band edges of InP with the potentials of E(InP/In^0) and RHE.

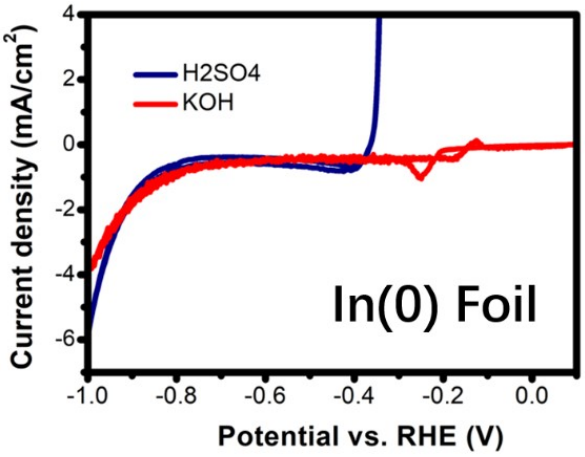

Figure S30. Comparison of CV of an In metal electrode in contact with 1.0 M H_2SO_4(aq) and 1.0 M KOH(aq), demonstrating slow HER kinetics at both pH = 0 and 14. Scan rate: 20 mV s^{-1}.

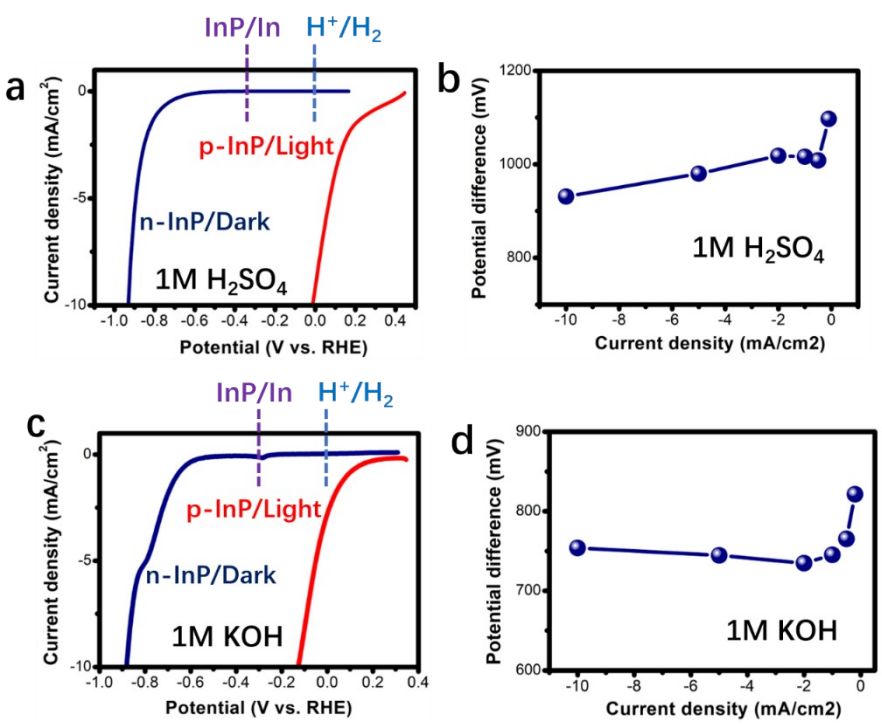

Figure S31. (a,c) Comparison of linear sweeps of n-InP electrodes in the dark to sweeps of illuminated p-InP electrodes (1 sun) in contact with (a) 1.0 M H_2SO_4(aq) and (c) 1.0 M KOH(aq). The scan direction was from positive to more negative potentials (scan rate: 50 mV s^{-1}). (b,d) Potential differences between the n-InP dark electrodes and p-InP photoelectrodes at mutually the same current densities in (b) 1.0 M H_2SO_4(aq) and (d) 1.0 M KOH(aq). For etched p-InP under 1-sun illumination, the potential required to produce -1 mA cm^{-2} of current density was +0.23 V vs RHE and +0.085 V vs RHE in 1.0 M H_2SO_4(aq) and 1.0 M KOH(aq), respectively. Comparison of linear sweeps of n-InP dark electrodes and illuminated p-InP electrodes revealed positive shifts in E from n-InP (dark) to p-InP (light) of >900 mV in 1.0 M H_2SO_4(aq) and of >750 mV in 1.0 M KOH(aq).

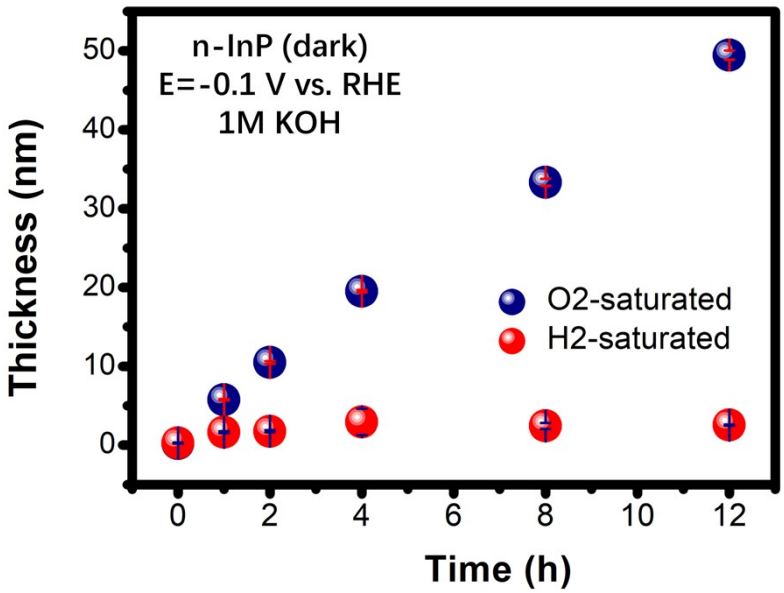

Figure S32. Comparison of corrosion thicknesses of n-InP electrodes (dark) held at E=-0.1 V vs. RHE over time, in 1.0 M KOH(aq) saturated with 1 atm of H_2(g) or O_2(g). The n-InP electrode exhibited a corrosion rate of ~4 nm h^{-1} in the O_2-saturated 1.0 M KOH(aq) electrolyte. These comparative experiments were performed outside the glovebox using a two-compartment electrochemical cell. These results confirmed that additional corrosion pathways of InP might arise upon exposure to dissolved oxygen.

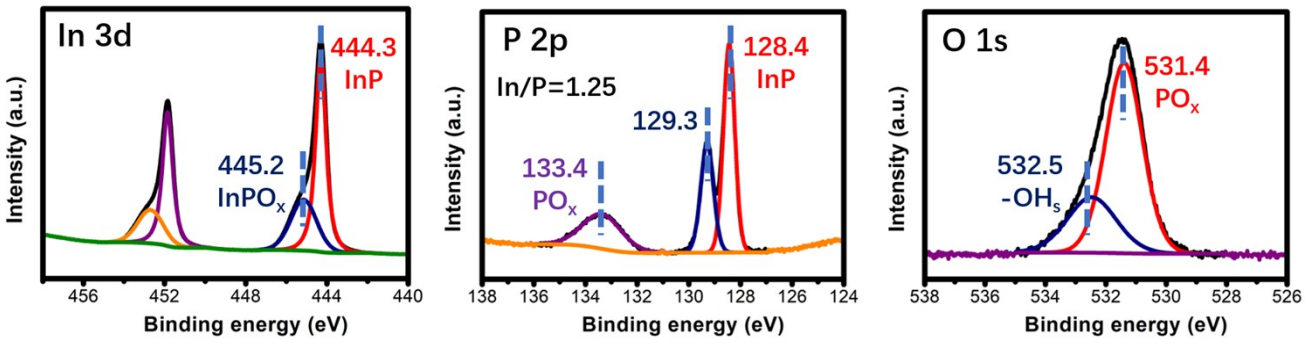

Figure S33. XPS data of p-InP with native oxide ($InPO_x$). Besides the peaks of InP, the distinct peak at high BE=445.2 eV in the In 3d region corresponds to native oxide ($InPO_x$). The peaks at BE=133.4 eV in the P 2p region, and 531.4 eV in the O 1s region are attributed to surface phosphate (PO_x).

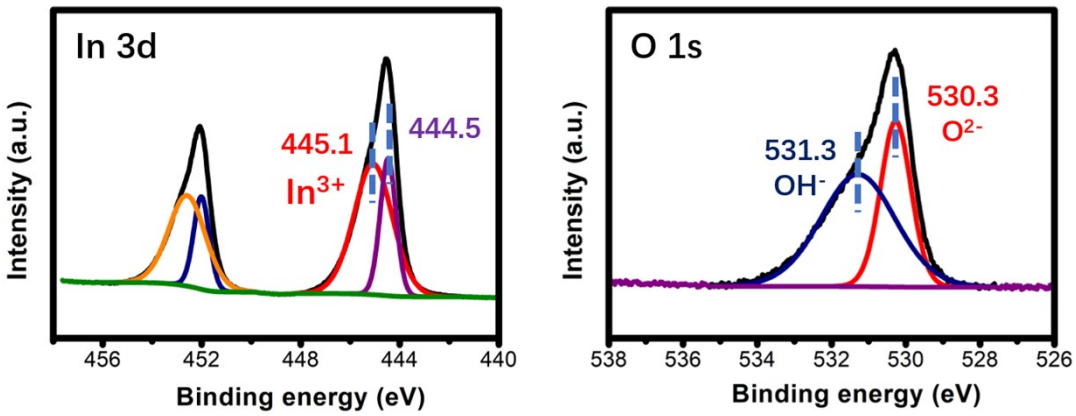

Figure S34. XPS data of cleaned indium tin oxide (ITO). Before XPS analysis, the ITO sample was cleaned by sonication in acetone, methanol and water (in order) for 5 min. The peaks at BE=444.5 eV and 445.1 in the In 3d region are assigned to InO_x. The peaks at BE=530.3 eV and 531.3 eV in the O 1s region are attributed to oxide (O^{2-}) and surface hydroxyl (OH^-), respectively.

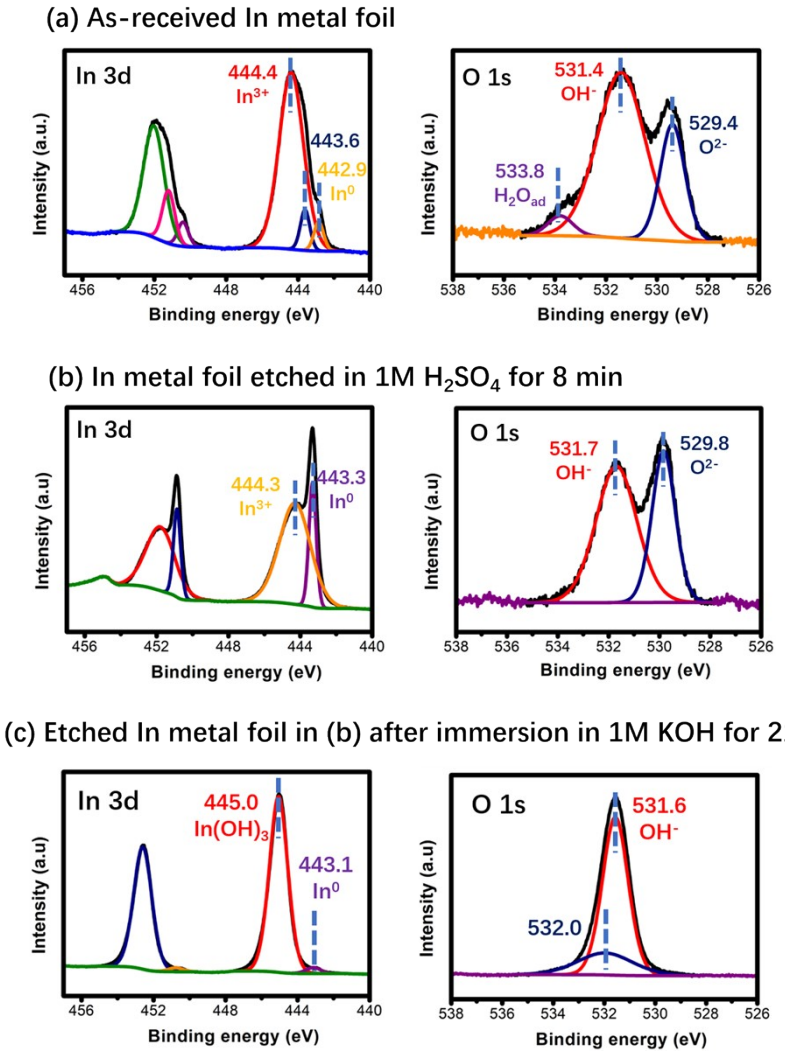

Figure S35. Comparison of XPS data for (a) as-received In metal foil, (b) In metal foil etched in 1.0 M H_2SO_4(aq) for 8 min and (c) etched In metal foil in (b) immersed in 1.0 M KOH(aq) for 21 h. In (a), the peaks at low BE=442.9 eV and 443.6 eV in the In 3d region are assigned to metallic In^0; the large peak at BE=444.4 eV is assigned to native oxide; the peaks at BE=529.4, 531.4 and 533.8 eV in the O 1s region are assigned to surface oxide (O^{2-}), hydroxyl (OH^-) and adsorbed water (H_2O_{ad}), respectively. In (b), the peak of metallic In^0 at BE=443.3 eV became much larger compared with the other peak at BE=444.3 eV assigned to surface oxide/hydroxide, indicating removal of native oxide by acid etching; the peaks at BE=529.8 and 531.7 eV in the O 1s region are assigned to surface oxide (O^{2-}) and hydroxyl (OH^-), respectively. In (c), the large peak at BE=445.0 eV in the In 3d region and the peak at BE=531.6 eV are attributed to $In(OH)_x$, suggesting the conversion of metallic In^0 into $In(OH)_x$ by prolonger immersion in 1.0 M KOH(aq).

Table S1. Standard Electrode Potentials in Aqueous Electrolytes at 25 °C for InP in V vs. RHE.[24,25]

Equilibria in 1.0 M H_2SO_4 (aq):	*E^0 (V vs. RHE)*
$In^{+3} + 3e^- \rightleftarrows In$	− 0.342
$H_3PO_3 + 6\,H^+ + 6e^- \rightleftarrows PH_3 + 3H_2O$	− 0.282
$H_3PO_4 + 2H^+ + 2e^- \rightleftarrows H_3PO_3 + H_2O$	− 0.276
$2H^+ + 2e^- \rightleftarrows H_2$	0.000
Equilibria in 1.0 M KOH (aq):	
$HPO_3^{-2} + 5H_2O + 6e^- \rightleftarrows PH_3 + 8OH^-$	− 0.480
$PO_4^{-3} + 2H_2O + 2e^- \rightleftarrows HPO_3^{-2} + 3OH^-$	− 0.291
$In_2O_3 + 3H_2O + 6e^- \rightleftarrows 2In + 6OH^-$	− 0.190
$In(OH)_3 + 3e^- \rightleftarrows In + 3OH^-$	− 0.172
$2H_2O + 2e^- \rightleftarrows H_2 + 2OH^-$	0.000

Table S2. Summary of experimental results of InP stability tests under varied conditions.

Sample	Electrolyte	E	light/ dark	Duration	In/P	In[a] $3d_{5/2}$	P[a] 2p	O[a] 1s	Pt[a] $4f_{7/2}$	PO_x[a,b]
		$V_{vs\ RHE}$		h	ratio	eV	eV	eV	eV	at %
n-InP	N/A	N/A	N/A	0	1.2	444.1, 444.7	128.3, 129.1, 132.6	529.5, 531.1, 532.6		8
p-InP	N/A	N/A	N/A	0	1.3	444.1	128.4, 129.2			
n-InP	H_2SO_4	-0.1	dark	48	1.2	444.1	128.3, 129.1	532.2		0
n-InP	H_2SO_4	-0.1	dark	24	1.2	444.3	128.5, 129.4, 133.3	532.8, 531.5		3
n-InP	H_2SO_4	-0.1	dark	10	1.1	444.2	128.4, 129.3	531.8, 532.6		0
p-InP	H_2SO_4	0	light	2	3.2	443.3, 444.1, 444.3	128.3, 129.2, 132.9	529.7, 531.4		8
n-InP	KOH	-0.1	dark	48	1.4	444.2, 444.8	128.3, 129.2, 132.7	531.3		4
n-InP	KOH	-0.1	dark	16	1.4	443.9, 445.2	128.1, 129	531.5		0
p-InP	KOH	-0.2	light	2	8.1	443.3, 443.9, 444.5	128.1, 128.9	529.6, 531.3		0
p-InP/Pt	N/A	N/A	N/A	as-prepared	1.1	444.3	128.5, 129.4, 132.7	531, 532.7	70.7, 71, 71.6	5
n-InP/Pt	H_2SO_4	-0.1	dark	50	1.2	444.3	128.4, 129.3, 132.2	530.7, 532.	70.5, 70.9, 72.2	5
p-InP/Pt	H_2SO_4	0	light	1	1.2	444.1	128.3, 129.2, 132.5	532.2, 530.7	70.5, 70.9, 72.4	5

p-InP/Pt	H_2SO_4	0	light	25	1.2	444.3, 445	128.5, 129.3, 133	531.8, 533.0	70.7, 71, 71.2, 72.9	5
p-InP/Pt	H_2SO_4	0	light	285	0.67	444.4	128.6, 129.5, 130.0, 132.6	532.3, 530.7	70.8, 71.1, 72.0	33
n-InP/Pt	KOH	-0.1	dark	48	1.2	444.1	128.3, 129.2, 132.3	531, 532.9	70.5, 71, 71.8	6
p-InP/Pt	KOH	0	light	72	3.1	444.2, 444.8	128.5, 129.4, 132.5	531.7, 529.9	71.2, 71.7	18
p-InP/Pt	KOH	N/A	light	3CVs	1.3	444.4	128.5, 129.4, 133	533, 531.1	70.8, 71.3	13
p-InP/Pt	KOH	0	light	15hr, then H_2SO_4	1.2	444.4	128.6, 129.4, 133	531.7	70.9, 71.3	16

[a] Binding energy all relative to C 1s at 284.8 eV

[b] at.% represents the percentage of P as PO_x relative to detected P atoms.

Table S3. A summary of key experimental results.

Electrode	Medium	E/V vs. RHE	In^0	Surface species	In/P	Decreased $\|J\|$ during CA	Dissolution of In ions
p-InP	H_2SO_4	0	Yes	InO_x	3.2	Yes	Yes
	KOH	-0.2	Yes	InO_x	8.1	Yes	No
p-InP/Pt	H_2SO_4	0	No	PO_x, P^0	0.67	No	Yes
	KOH	0	No	InO_x, PO_x	3.1	Yes	No
n-InP	H_2SO_4	-0.1	No	No	1.2		Yes
	KOH	-0.1	No	$In(OH)_x$	1.4		No
n-InP/Pt	H_2SO_4	-0.1	No	No	1.2		Yes
□	KOH	-0.1	No	No	1.2	□	No

Table S4. Criteria of XPS peak assignments for different In-containing species.[10–22]

Species	**In $3d_{5/2}$/eV**	**O 1s/eV**	**In/P ratio**
InP	444.2±0.2	N/A	1.2
$In(OH)_x$	444.9±0.2	531±0.5	>1.2
$InPO_x$	444.9±0.2	531±0.5	~1.2
InO_x	444.9±0.2[a]	530±0.5	>1.2

[a]XPS data of the In metal foils showed slightly lower values (444.3-444.4 eV) for surface oxide (InO_x) over metallic In^0, compared with ITO and other literature data.

References

1 K. Liu, J. C.-C. Yu, H. Dong, J. C. S. Wu and M. R. Hoffmann, *Environmental Science & Technology*, 2018, **52**, 12667–12674.

2 Y. Lin, R. Kapadia, J. Yang, M. Zheng, K. Chen, M. Hettick, X. Yin, C. Battaglia, I. D. Sharp, J. W. Ager and A. Javey, *J. Phys. Chem. C*, 2015, **119**, 2308–2313.

3 K. Sun, Y. Kuang, E. Verlage, B. S. Brunschwig, C. W. Tu and N. S. Lewis, *Advanced Energy Materials*, 2015, **5**, 1402276.

4 E. R. Corson, E. B. Creel, Y. Kim, J. J. Urban, R. Kostecki and B. D. McCloskey, *Review of Scientific Instruments*, 2018, **89**, 055112.

5 J. D. Benck, S. C. Lee, K. D. Fong, J. Kibsgaard, R. Sinclair and T. F. Jaramillo, *Adv. Energy Mater.*, 2014, **4**, 1400739.

6 J. Gu, J. A. Aguiar, S. Ferrere, K. X. Steirer, Y. Yan, C. Xiao, J. L. Young, M. Al-Jassim, N. R. Neale and J. A. Turner, *Nature Energy*, 2017, **2**, 16192.

7 S. M. Thalluri, B. Wei, K. Welter, R. Thomas, V. Smirnov, L. Qiao, Z. Wang, F. Finger and L. Liu, *ACS Energy Lett.*, 2019, **4**, 1755–1762.

8 I. A. Moreno-Hernandez, S. Yalamanchili, H. J. Fu, H. A. Atwater, B. S. Brunschwig and N. S. Lewis, *J. Mater. Chem. A*, 2020, **8**, 9292–9301.

9 X. Zhou, R. Liu, K. Sun, D. Friedrich, M. T. McDowell, F. Yang, S. T. Omelchenko, F. H. Saadi, A. C. Nielander, S. Yalamanchili, K. M. Papadantonakis, B. S. Brunschwig and N. S. Lewis, *Energy & Environmental Science*, 2015, **8**, 2644–2649.

10 Z. M. Detweiler, S. M. Wulfsberg, M. G. Frith, A. B. Bocarsly and S. L. Bernasek, *Surface Science*, 2016, **648**, 188–195.

11 R. Bayón, C. Maffiotte and J. Herrero, *Thin Solid Films*, 1999, **353**, 100–107.

12 T. Hu, H. Li, Z. Liang, N. Du and W. Hou, *Journal of Colloid and Interface Science*, 2019, **545**, 301–310.

13 W. Zhu, J. Zhai, Z. Sun and L. Jiang, *J. Phys. Chem. C*, 2008, **112**, 8338–8342.

14 Z. M. Detweiler, J. L. White, S. L. Bernasek and A. B. Bocarsly, *Langmuir*, 2014, **30**, 7593–7600.

15 D. V. Shinde, D. Y. Ahn, V. V. Jadhav, D. Y. Lee, N. K. Shrestha, J. K. Lee, H. Y. Lee, R. S. Mane and S.-H. Han, *J. Mater. Chem. A*, 2014, **2**, 5490–5498.

16 J. L. White and A. B. Bocarsly, *J. Electrochem. Soc.*, 2016, **163**, H410–H416.

17 L. B. Hoch, L. He, Q. Qiao, K. Liao, L. M. Reyes, Y. Zhu and G. A. Ozin, *Chem. Mater.*, 2016, **28**, 4160–4168.

18 A. Hofmann, P. Streubel and A. Meisel, *Surf. Interface Anal.*, 1988, **12**, 315–319.

19 B. Glorieux, R. Berjoan, M. Matecki, A. Kammouni and D. Perarnau, *Applied Surface Science*, 2007, **253**, 3349–3359.

20 H. Virieux, M. Le Troedec, A. Cros-Gagneux, W.-S. Ojo, F. Delpech, C. Nayral, H. Martinez and B. Chaudret, *J. Am. Chem. Soc.*, 2012, **134**, 19701–19708.

21 S.-T. Jean and Y.-C. Her, *CrystEngComm*, 2011, **13**, 2324.

22 H. J. Lewerenz and K. H. Schulte, *Electrochimica Acta*, 2002, **47**, 2639–2651.

23 A. Jain, S. P. Ong, G. Hautier, W. Chen, W. D. Richards, S. Dacek, S. Cholia, D. Gunter, D. Skinner, G. Ceder and K. A. Persson, *APL Materials*, 2013, **1**, 011002.

24 M. Pourbaix, *Atlas of electrochemical equilibria in aqueous solutions*.

25 A. J. Bard, R. Parsons and J. Jordan, *Standard potentials in aqueous solution*, CRC press, 1985,

vol. 6.